Influence of salt concentration on charge transfer when a water front moves across a junction between a hydrophobic dielectric and a metal electrode

L.E. Helseth

Department of Physics and Technology, Allegaten 55, 5020 Bergen, University of Bergen, Norway

Email: Lars.Helseth@ift.uib.no

ABSTRACT: An energy harvesting device based on water moving across the junction between a hydrophobic dielectric and a metal electrode is demonstrated. The charge transfer due to contact electrification as the junction is dipped vertically into water is investigated. Experiments combined with finite element simulations reveal how the electrode voltage changes during the dipping process. Moreover, the charge transfer observed for a range of salt concentrations is studied, and it is found that there exists an optimal salt concentration which allows maximum charge transfer. It is suggested that these results can be understood as due to the additional charge removal from the diffuse electrical double layer at the hydrophobic surface. It is demonstrated that by tuning the salt concentration, one can harvest more than three times the electrical power as compared with pure water.

KEYWORDS: Charge transfer, contact electrification, water, energy harvesting

Introduction

Electrification of water occurs naturally when its surface is altered, and this phenomenon has been investigated for more than a century [1-7]. Water droplets are known to acquire charge from the environment, which has been related to CO_2 gas in the atmosphere as well as infrared radiation [8]. The charge of water droplets can be tuned depending on such factors as the electric field [9], the chemical composition of the liquid [10], the chemical composition of the substrate [11] or the triboelectric history of the substrate it comes in contact with [12]. When water is contacted by hydrophobic surfaces such as fluoropolymers, a negative charge is acquired by the solid surface [13-16], often attributed to the preferential adsorption and/or orientation of O-H groups [17-21]. The amount of charge left behind after the water has passed the hydrophobic substrate has recently been explained by a transfer coefficient [22]. Research has also revealed that leaching of ions may influence the surface charge significantly [23], thus making it important to separate inert and noninert surfaces.

The charge that develops when water comes in contact with solid substrates can be utilized in various manners. For example, water flow allows the removal of loosely bound ions in the electrical double layer near the substrate surface, giving rise to a streaming current which can be used to harvest electrical energy [24-27]. More recently, contact electrification due to intermittent contact between solid surfaces and water droplets or moving wave fronts has been utilized for harvesting energy [28-45]. Self-powered sensors for fluids, utilizing for example ion specificity [46] or coalescence [47] have attracted considerable attention. Water-powered remote transfer of kinetic energy represents a new type of actuator that may have impact on future small-scale devices [48]. Comprehensive reviews of water-solid triboelectric nanogenerators can be found in Refs. [49,50].

Very recently, it has been demonstrated that a polymer-metal junction featuring a front electrode coming in contact with water may provide increased electrical performance for wave [51] and water droplet [52] energy harvesting. However, the influence of salt concentration on the performance of such devices has not been studied in detail. In general, it appears that the influence of added ions on charge transfer is not

well understood for a range of energy harvesting devices. Here, the working mechanism of such a front-electrode device is investigated, and it is explained why one obtains a significant increase in charge transfer and electrical power when adding small amounts of salt.

Experimental setup

In this study, a double electrode device was made by attaching 0.03 mm thick aluminum tape to approximately 50 mm tall, 20 mm wide and 2 mm thick polystyrene substrate. A few of the initial experiments were also done without the substrate (with only aluminum sheets or films in the middle acting as electrodes and support) and with other types of plastic substrates, obtaining the same experimental results as with the described substrate. The substrate therefore had no other function than as support for the thin aluminum film. Fluorinated ethylene propylene (FEP) of thickness 50 μm (Dupont) was attached with adhesive to the aluminum film, thus covering the entire metal. The adhesive used was either acrylic adhesive or cured polydimethylsiloxane (PDMS, Sylgard 184). Small amounts of PDMS, with curing agent to elastomer ratio 1:10 heated to 100° C for 10 min, was used to fill the openings between FEP and metal, in order to ensure that no water could come in contact with the aluminum when the device was dipped into water. The electrical resistivity of the PDMS seal was tested before and after use to ensure that water did not leak through it. This metal electrode, which was covered by FEP and some minor amount of PDMS, is hereafter denoted the back-electrode. A front-electrode made of 0.03 mm thick aluminum was then attached to the FEP using either acrylic adhesive or PDMS. The edge of the front-electrode was placed 15 mm above the lower edge of the back-electrode, but otherwise the two electrodes covered similar area separated by an FEP film. A picture of the single and double-electrode device is shown in Fig. 1 c), along with a picture of parts of the experimental setup.

The single-electrode device functioned in this study mainly as a reference, as its working mechanism has been elaborated in other studies [29,32,33,42]. It was made using the same procedure as the double-

electrode device, except that the front-electrode was not mounted, and the edge of the lower back-electrode was lifted 2 cm up on the substrate such that the FEP film covered it smoothly.

At this point it should be emphasized that the idea of using a front-electrode was already promoted in Refs. [51,52]. Here, the working mechanism of a front-electrode device is further studied, both from an electrostatic and electrochemical perspective, and it is demonstrated how its performance can be enhanced.

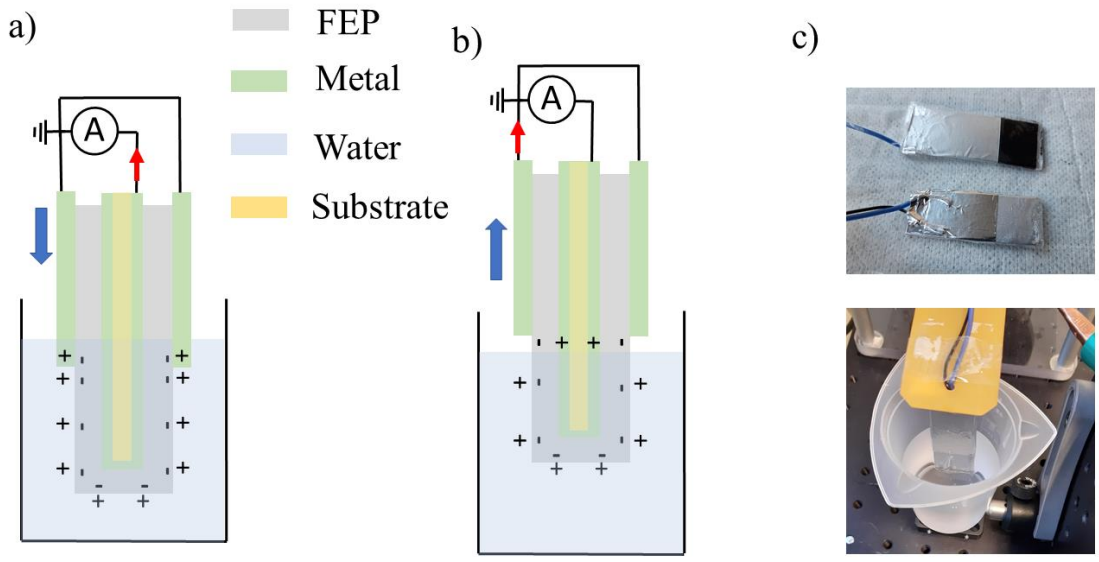

Figure 1. Simplified schematic drawing of the electrification as the double-electrode device is dipped into a) or withdrawn from b) water. The picture c) shows a single-electrode device and a double-electrode device (upper) as well as the experimental setup (lower). The front-electrode comes in contact with water, while the back-electrode does not come in contact with water.

The liquid used here was deionized water without or with added NaCl (Sigma Aldrich). As starting point ultrapure water (18.2 MΩcm, Millipore) was allowed to rest in plastic container in air, thus giving a resistivity of the order of 1 MΩcm which will here be referred to as pure water. The water, with or without

salt, was poured into a polystyrene beaker to a fixed liquid level of 70 mL. The FEP surface was hydrophobic for both advancing and receding contact lines as the device was dipped into and pulled out of water. On the other hand, the aluminum film was hydrophilic for both advancing and receding contact lines. The wetting properties of both FEP and aluminum were reported in Refs. [39,53].

The single and double-electrode devices were mounted on a cantilever and dipped into water using an electromagnetic shaker (Smart Materials GmbH), see also Ref. [39]. The amplitude and frequency of the oscillations with which the single and double-electrode devices were dipped into water could be controlled. To ensure consistency, a frequency f = 5 Hz and an amplitude (from equilibrium) 1 cm was selected here unless otherwise stated. The position of the transition between the front-electrode and FEP was kept constant between experiments by adjusting the water level using a precision translation stage. The voltage, current and charge was measured using a Keithley 6514 instrument.

Electrical characterization

In the following, the working mechanism of the double-electrode device is described in detail. The single electrode device has been described in detail in the literature [29,32,33,42], and will therefore only be used as a reference in this study. The basic contact electrification and electrostatic induction process is shown in Fig. 1. The FEP surface becomes negatively charged when put in contact with water [54]. In pure water, the negative charges are likely OH-ions. This negative charge attracts counterions forming an electrical double layer while the FEP surface is immersed. The part of the FEP surface that is above water does not attract countercharge from the water. However, the positive charge will be attracted by the negative FEP-surface charge density in the back-electrode not in contact with water, thus keeping the electrical potential of this electrode low. When the double-electrode device is lowered so much that also the front electrode comes in contact with water, the potential of the back electrode is increased and there is a corresponding current from the back to the front-electrode as shown in Fig. 1 a). Upon rising the front-electrode out of the water, the current reverses as shown in Fig. 1 b).

In order to understand how the potential difference between the two electrodes changes as the double electrode is dipped into water, electrostatic finite element modelling in COMSOL 5.4 was undertaken assuming an FEP surface charge density -0.35 μC/m^2 and the front electrode grounded. This particular surface charge density was found to provide the best fit of the numerical model to the experimental data. Any space charges were neglected, and the electrostatic problem was solved numerically using the Poisson equation with the boundary conditions stated above. Convergence of the numerical solutions were ensured by gradually refining the mesh until the variations in the potential between different simulations were below 0.1 V.

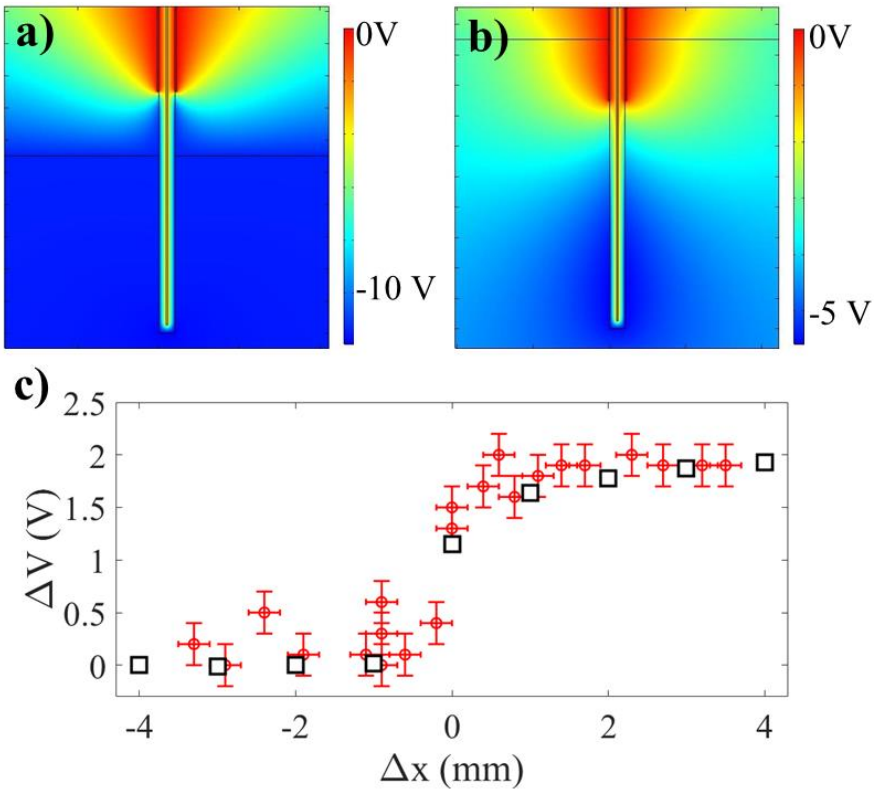

Figure 2. Finite element electrostatic simulations when the earthed front-electrode is out of a) or in b) pure water with FEP surface charge density -0.35 μC/m^2. The water level is represented by a thin horizontal, black line. In c), the measured (red circles) and modelled (black squares) change in open circuit potential is displayed.

Figure 2 a) shows the electrical potential distribution when the double-electrode plate is dipped into water such that only the FEP is in contact with water, whereas Fig. 2 b) shows the potential distribution when also the front-electrode comes in contact with water. As explained above, the potential of the back-electrode increases as the front-electrode is inserted into water. The red circles in Fig. 2 c) show the change ΔV in open circuit electrical potential between the back and front-electrodes when the device is dipped into water. Note that the front electrode is grounded, and therefore held at zero potential. The position $\Delta x=0$ mm corresponds to the position where the front-electrode just comes into contact with water. The potential is measured in steps from the position where the front-electrode is lifted about 4 mm out of the water ($\Delta x=-4$ mm) until it is immersed 4 mm into the water ($\Delta x=4$mm). Between each step, the open circuit potential is allowed to equilibrate for about 30 seconds before the potential measurement is recorded. As long as there is a constant surface charge density on the FEP surface, the measured potential difference remains constant. FEP is a known electret with abilities to stay charged even under humid conditions, and there are many ways in which a relatively constant surface charge can be implemented, including ion injection and triboelectrification. If one increases the dipping speed, tribocharging of the FEP surface results in a larger surface charge density, and therefore also a larger voltage. In principle, any splashing or unintended additional movement of the FEP surface in and out of water would alter the surface charge density. It is crucial that the experiments are undertaken at controlled dipping speeds or at quasi-static conditions in order to obtain repeatable results. In the experiments reported in Fig. 2 c) the dipping speed was kept close to zero, and the constancy of the measured voltage during equilibration suggested that the surface charge density did not change during the experiments. As the front electrode is very slowly immersed into water, a steep increase in potential on the back-electrode of about 2 V can be observed, as seen in Fig. 2 c). The finite element simulations of Fig. 2 c) are in agreement with the experimental data, thus suggesting that the observed sharp increase in voltage is well explained by these electrostatic simulations.

In the rest of the experimental results reported in this work, the single and double electrode devices were vibrated back and forth into the water at a frequency f=5 Hz. In the case of the single electrode device, the vertical position was selected such that the edge of the back-electrode was leveled with the water surface at maximum velocity (i.e. when the cantilever is horizontal). In the case of the double-electrode, the edge of the front-electrode was leveled with the horizontal water surface when the cantilever had maximum velocity. The cantilever oscillated with amplitude of about z_0=1.0 cm, and the velocity changed harmonically according to $v=2\pi f z_0 \sin(2\pi f t)$, which gives a maximum velocity of $2\pi f z_0 \approx 0.3$ m/s at f=5Hz. The left trace in Fig. 3 a) shows the current generated in the single electrode device when vibrated into pure water, whereas the right trace shows the current in 1 mM NaCl. As can be seen, the current peaks are about 0.5 μA in pure water, but increase slightly when a small amount of salt is added. Figures 3 b)-d) show current, voltage and absolute value of the charge of a double electrode device that is vibrated into the liquid at the same velocity and amplitudes as for the single electrode device. In all cases the left trace corresponds to pure water, whereas the right trace corresponds to 1 mM NaCl. A few interesting features can be observed here. First, it is found that moving the double-electrode up and down at a frequency of f = 5 Hz generates changes in potential of about 15 V in pure water, which is much larger than the 2 V reported in Fig. 2. It is found that fast movement enhances the charge transfer, thus building up larger potential differences than those reported in Fig. 2. As such, the experimental data and simulations reported in Fig.2 only represent the quasi-static equilibrium situation, and are not very helpful when it comes to understanding influence of dynamics or ions on charge transferred.

In Fig. 3 it is seen that the current increases significantly on going from the single to the double electrode device. Moreover, introducing a small ion concentration in the solution seems to enhance the current and the charge transfer, as will be discussed in more detail in the next section.

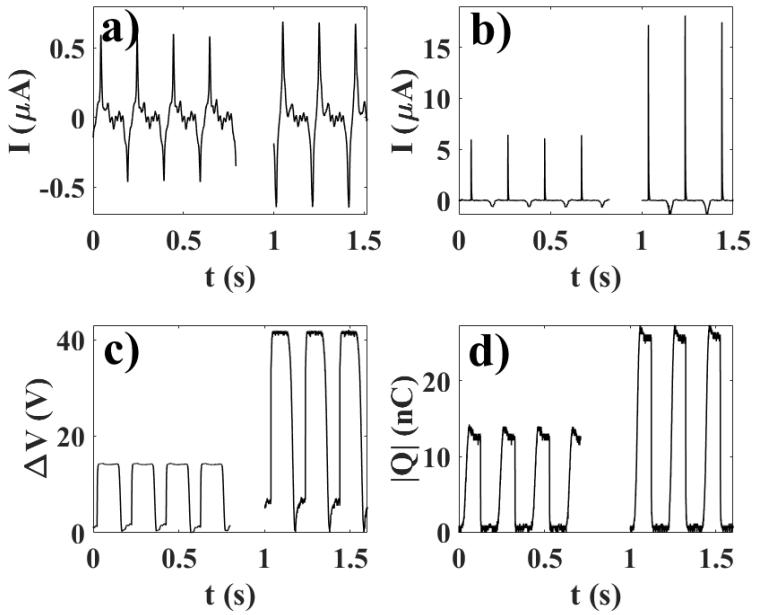

Figure 3. The current a) of a single electrode in pure water (left trace) and 1 mM NaCl (right trace). The current b), change in voltage c) and charge transfer d) of a double electrode in pure water (left trace) and 1 mM NaCl (right trace).

Upon comparing Figs. 3 a) and b), it is seen that the shapes of the current traces for a double-electrode device differ significantly from those of the single-electrode device. The single-electrode current trace is almost symmetric and a positive pulse lasts about 40 ms. The dynamics of the charge transfer under such circumstances has been elaborated in Refs. [39,55], and similar considerations apply here. On the other hand, the double-electrode current trace is highly asymmetric with a large positive current pulse lasting about 5 ms when the front-electrode meets water, followed by slower negative current that lasts near 40 ms when the front-electrode is dragged out of water, a dynamics similar to that found in Ref. [56]. It should be mentioned that the absolute value of the charge transfer is the same in both positive and negative current pulses. Although no simulations or detailed explanation of the time dynamics are offered in this work, it is reasonable to assume that the larger positive current when the front-electrode meets water is due to the accumulated charge near the hydrophobic surface as it is lowered. When the hydrophilic metal

is moved out of the water, the charge transfer is not that sudden due to the adhesion of water to the metal surface causing a longer period for the charge transfer to occur.

Of interest in applications is the electrical power that can be extracted in an external load. Here, only the double-electrode device is considered, since this type of device is new, provides more power and it is of interest to characterize its performance. To get an impression of the available power from a double-electrode device, the current I was measured with the amperemeter connected in series with an external resistor R. The peak current I_p when the front electrode meets water is shown in fig. 4 a) as red squares when pure water was used. The black circles correspond to 1 mM NaCl. As in Fig. 3 b), it is seen that the current increases when a small amount of salt is added. The power is found using $P_p=RI_p^2$, and is given in Fig. 4 b) for pure water (red circles) and 1 mM NaCl (black squares). Here R_p is the internal resistance of the device. In Fig. 4), the black dashed lines are nonlinear fits of $I_p=V_0/(R+R_i)$ and $P_p=RI_p^2$ to the experimental data for 1 mM NaCl with $R_i = (2.6 \pm 0.4)$ MΩ and $V_0 = (43 \pm 2)$ V, whereas the red dashed lines are fits to the experimental data for pure water with $R_i = (4.5 \pm 0.4)$ MΩ and $V_0 = (29 \pm 2)$ V. The reasonably good agreement between fits and experimental data suggest that the energy harvesting device can be represented by an internal impedance $R_i = (2.6 \pm 0.4)$ MΩ for 1 mM NaCl and $R_i = (4.5 \pm 0.4)$ MΩ for pure water. Note however that while the voltage V_0=43 V fits well with that measured in Fig. 3 c) for 1 mM NaCl, the V_0=29 V found for pure water does not compare that well with the 15 V found in Fig. 3 c). The reason for this discrepancy is not known at this point.

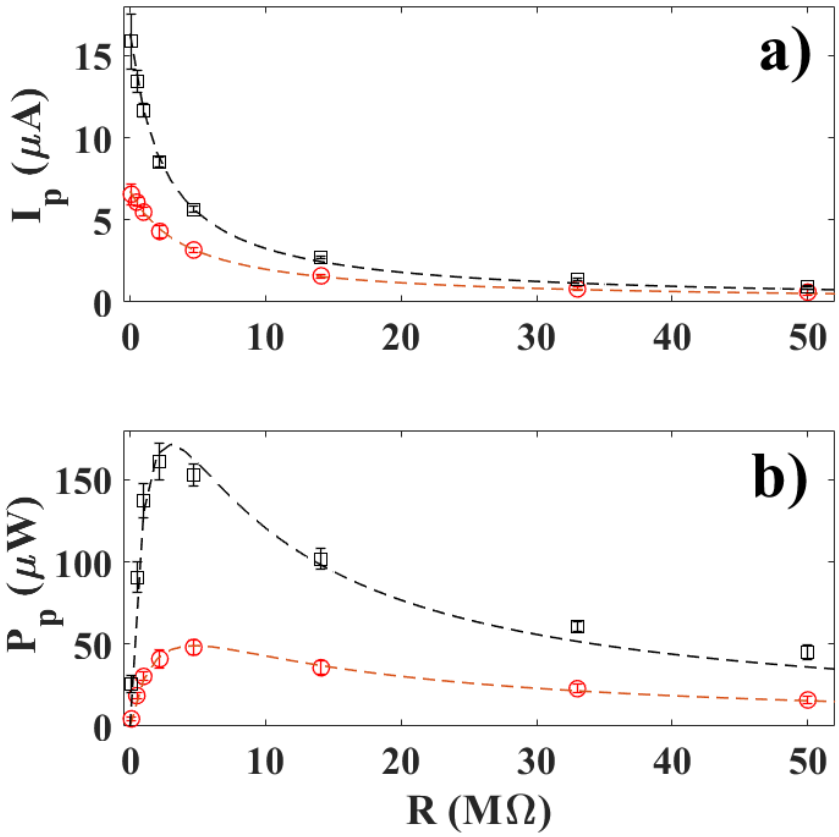

Figure 4. The peak current I_p (a) and peak power P_p (b) as a function of load resistance R for pure water (red circles) and 1 mM NaCl (black boxes). Also shown as dashed lines are the corresponding nonlinear fits using $I_p=V_0/(R+R_i)$, and $P_p=RI_p^2$, where V_0 is the peak voltage and R_p is the internal resistance.

Salt concentration dependence

The dependence of the charge transfer on salt concentration was studied in more detail. In Fig. 3 d) it is seen that the maximum absolute value of the charge transferred when the double-electrode device is dipped into water changes from about 13 nC in pure water to about 25 nC in 1 mM NaCl. This maximum charge during dipping, corresponding to the integrated charge associated with a positive current pulse, was recorded as a function of salt concentration. Figure 5 shows the result for the double-electrode device (squares) and the single-electrode device (circles). The latter is included as a reference, to demonstrate that the general charge transfer behavior is not related to the application of a non-inert front-surface metal

electrode. It is seen that for the single-electrode device the transferred charge reached a maximum of about 12 nC at 1 mM NaCl, whereas the double-electrode device reached a maximum of 26 nC at 0.1 mM NaCl. Note that the variations in charge transfer in the double-electrode device were within the measurement error for both 1 mM and 0.1 mM, and it is therefore only possible to say that the maximum charge was found in the range between 0.1 and 1 mM NaCl. Similar considerations are valid also for the single-electrode device, but here the range wherein the peak could be was broader, from 0.1 mM to 10 mM. However, for both type of devices there is a clear indication that an optimal concentration exists, where the maximum amount of charge is transferred.

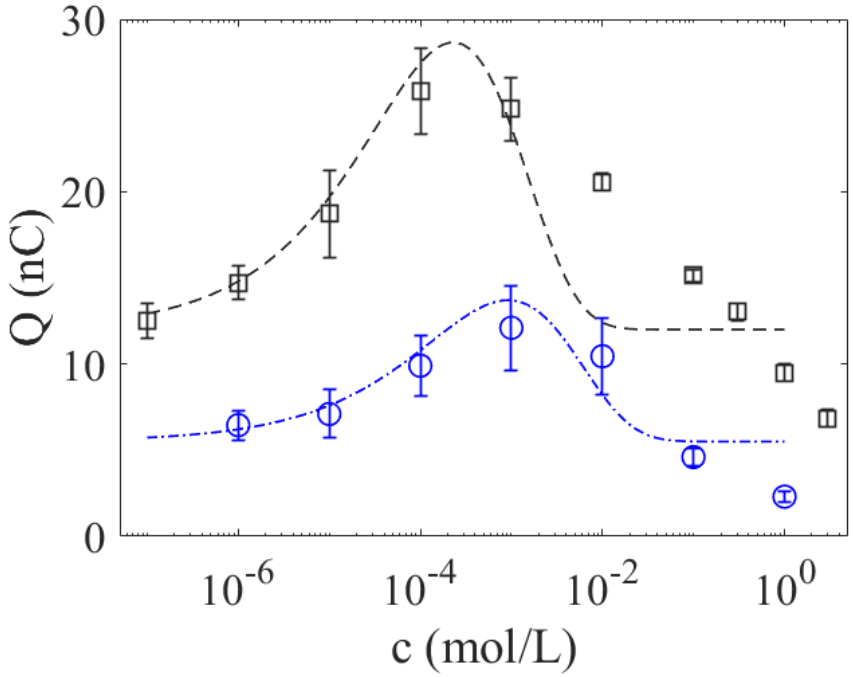

Figure 5. The charge Q for the double electrode cell (black squares) and the single electrode cell (blue circles) for different concentrations of salt (c). The dashed, black line is a theoretical fit of Eq. (7) to the data for the double electrode cell. The dash-dotted blue line is a theoretical fit of Eq. (7) to the data for the single electrode cell.

The results reported in Fig. 5 are in agreement with experimental results reported in the literature. For example, in Ref. [57] it was found that upon squeezing water droplets between a dielectric layer and a conducting substrate, the peak voltage would exhibit a maximum near 1 mM NaCl. In Ref. [58] it was found that pressing water droplets together followed by charge measurement resulted in an increase in charge with salt concentration up to about 0.01 mM – 0.1 mM, followed by a subsequent decrease in observed charge. Together, these studies suggest that increasing the ion concentration by a small amount increases the charge transfer, while too large ion concentration results in a weakened charge transfer. In Ref. [52] it was demonstrated that the performance of a front-electrode system could be enhanced by either injecting ions or by letting a large number of water droplets hit the surface, leading to charge pumping into the electrical double layer. Here, as in Ref. [22], such charge pumping is not actively promoted, and the currents and voltages reported are much smaller than that of Ref. [52]. However, it is demonstrated in the current work that the charge transfer in such a system can also be boosted using a small additional ion concentration in the liquid itself. It is argued that the observed enhancement in charge transfer can be explained by transfer of ions out of the electrical double layer during flow which subsequently are inducing additional charge in the electrodes.

In Ref. [58] it was argued that the very low ion concentration in pure water cannot fully support ion transfer at the liquid-solid interface, and that the charge transfer during contact electrification can be increased by facilitating this ion transfer process with more added ions. It was further argued that too large ion concentrations would lead to screening effects, thus reducing the charge transfer. In Ref. [58], contact electrification was attributed to electron transfer which occurred when water molecules came close to negatively charged groups on the hydrophobic surface. If this picture is correct, then coupling of electron transfer and ion absorption is essential for contact electrification between aqueous solutions and hydrophobic solids. However, verifying such an assumption experimentally would require direct measurements of electron transfer during liquid-solid contact, which is outside the scope of the current work.

In pure water, there is already a charge transfer Q_0 due to charges that are present even in absence of any external added salt (c=0 M). Extensive previous research has related this charge to preferential adsorption and/or orientation of O-H groups near the hydrophobic polymer surface [17-21]. However, it should also be pointed out that recent simulations seem to indicate that negative charge can also be accumulated due to asymmetries in the hydrogen bond network [59], thus pointing to a rather complex picture. In the absence of additional ions, it remains clear that only combinations of hydrogen and oxygen, including clusters thereof, can be responsible for the observed charge. It has been demonstrated that an increased charge transferred occurs in the presence of small additions of hydroxyl ions, thus suggesting that additional negative charge was contributed during contact electrification [56,58]. The aim of this work is not to identify the origin of the charge transfer in pure water, which is a particularly difficult task which can only be undertaken by a very thorough combination of ab-initio simulations combined with experimental investigations of molecular scale arrangements. Here, the charge transfer when dipping the device in pure water will be treated as a constant, Q_0. However, it is argued that the additional charge transfer observed when adding NaCl to the water can be explained by resorting to electrical double layer theory, since in fact this a much-applied theory used to explain the behavior of electrical double layers.

The charge near the solid surface is governed by a socalled Stern layer of adsorbed and immobile ions, followed by a diffuse and more mobile outer layer which in equilibrium often is assumed to be governed by Boltzmann statistics. If z is the ion valence number, the potential ϕ is found from the Poisson-Boltzmann equation for a one-dimensional system is [60]

$$\frac{d^2\phi}{dx^2} = -\frac{\rho}{\varepsilon\varepsilon_0} = \frac{2n_o ez}{\varepsilon\varepsilon_0}\sinh\left(\frac{ze\phi}{k_B T}\right) \quad , \qquad (1)$$

which has a solution

$$\tanh\left(\frac{ze\phi}{4k_BT}\right) = \tanh\left(\frac{ze\phi_d}{4k_BT}\right) e^{-\kappa x} \quad , \qquad (2)$$

where the inverse Debye length (λ_D) is given by

$$\kappa = \frac{1}{\lambda_D} = \sqrt{\frac{2n_0 z^2 e^2}{\varepsilon\varepsilon_0 k_B T}} \quad . \qquad (3)$$

Here the n_0 is the density of ions, e the electronic charge, ε_0 the permittivity of vacuum, ε the relative permittivity, k_B is Boltzmann's constant and T the temperature. The inner surface of the diffuse charge layer is assumed to have a fixed potential ϕ_D. Clearly, this assumption can be debated, but is here used to obtain a minimalistic theory that can aid further understanding of the data. Assuming ε=80 and room temperature (T=300 K), the inverse Debye length can be expressed in terms of the concentration c (moles per litre) as $\kappa = 3.3\sqrt{c}$ (nm^{-1}) [60]. For small potentials ($ze\phi/k_BT<<1$) or large potentials ($ze\phi/k_BT>>1$) one can express Eq. (2) as

$$\phi \approx Be^{-\kappa x} \quad , \qquad (4)$$

with $B = \phi_d$ in the former and $B = \frac{4k_BT}{ze}\tanh\left(\frac{ze\phi_d}{4k_BT}\right)$ in the latter case. The charge density in the diffuse charge layer is found using the Poisson-equation as

$$\rho = -\varepsilon\varepsilon_0 \frac{d^2\phi}{dx^2} = -B\kappa^2 e^{-\kappa x} \quad , \qquad (5)$$

When the fluid flows past the polymer surface, only a certain amount of the charge is dragged along by the stress. The coupled hydrodynamic flow and charge mobility is a complex problem, where the mobility of the charge and the slip length are key parameters that play out differently for hydrophilic and hydrophobic surfaces [61-63]. The contribution of the stagnant layer to the charge dynamics near a hydrophobic surface has to the knowledge of the author not been reported in the literature for systems similar to that under study. However, it is reasonable to assume that a certain amount of charge is left behind [22,64], which means that an immobile charge layer plays a role also in the charge transfer reported in this study. The charge left behind on a polymer surface has been explained by assuming a stagnant layer leaving a certain amount of the diffuse charge [64]. To explain the experimental observations in the current study, it is assumed that the stagnant layer ends at some distance $x=x_s$, and that only space charge beyond that region is transported towards the electrode. As these charges are removed by fluid flow, there is a corresponding triboelectrification that induces charge ΔQ in the electrodes that is proportional to the amount of charge ΔQ_1 removed. The additional charge ΔQ_1 per area transported due to the added salt is found by integrating the charge density from x_s to infinity, i.e.

$$\Delta Q_1 = \int_{x_s}^{\infty} \rho(x) dx = \int_{x_s}^{\infty} -\varepsilon_0 \varepsilon \frac{d^2\varphi}{dx^2} dx = -B\varepsilon_0 \varepsilon \kappa e^{-\kappa x_s} \quad , \quad (6)$$

where $\Delta Q = A\Delta Q_1$ and A is the hitherto unknown constant proportional to the area over which the charge is gathered by the electrode. The horizontal width of the electrode is w, and a corresponding vertical stripe of unknown effective height L is assumed to participate in charge collection, thus giving A=wL. Since the Stern layer is assumed to be negatively charge, one has B<0, such that there are positive counterions in the diffuse layer contributing with $\Delta Q>0$. Under the assumption of $\varepsilon=80$ and room temperature (T=300 K), the expression for the total charge can be given as

$$Q = Q_0 + \Delta Q \approx Q_0 - 2.3AB\sqrt{c}e^{-3.3\sqrt{c}x_s} \quad , \quad (7)$$

with x_s given in nanometers. The theory suggests that there are three regions of charge transfer. First, when the salt concentration is very small ($c<<0.1$ mM) the charge transfer is governed by the contact electrification with water alone as described by Q_0 discussed above. Increasing the salt concentration decreases the Debye length and increases the charge available to be transported away until the maximum charge transfer occurs when $c_{max}=1/(3.3x_s)^2$. Experimentally, this occurs in the region 0.1-1.0 mM. As the salt concentration is increased even further, the electrical double layer eventually contract so much that no additional ions can be transported and the charge is once again dominated by Q_0. In Fig. 5 the dashed, black line shows a fit of Eq. 7 to the experimental data for the double-electrode device with $Q_0=12$ nC, $AB=-1.3\cdot10^{-6}$ Vm^2 and $x_s=20$ nm. If one assumes that B=-0.1 V (as it would be for large ion concentrations), the area calculated is $A=1.3\cdot10^{-5}$ m^2. Since $w=1.0\cdot10^{-2}$ m, one gets $L=1.3\cdot10^{-3}$ m for the vertical length over which charge is collected, which appears reasonable given the thickness 0.1 mm of the front aluminum electrode and the geometry of the system. The obtained thickness for the stagnant layer, $x_s=20$ nm, is in the range of the typical diffuse electrical double layer thicknesses at low concentrations, and is therefore reasonable. In Fig. 5 the dash-dotted blue line shows a fit of Eq. 7 to the experimental data for the single-electrode device with $Q_0=5.5$ nC, $AB=-0.3\cdot10^{-6}$ Vm^2 and $x_s=10$ nm. The charge Q_0 for the double-electrode is approximately two times that of the single-electrode, which is most likely due to charge pumping back into the electrical double layer, although the exact origin cannot be determined from the available data. The effective area A is also smaller if one assumes that B remains the same, which might be due to a larger separation between the adsorbed charge and the back-mounted electrode, such that the electrostatic interaction is weaker and a smaller effective height L participates in the charge collection. Finally, the thickness of the stagnation layer is smaller for a single-electrode than for a double-electrode, but they are still within the same order of magnitude. It is not clear at this point how the presence of the metal alters the stagnation layer thickness.

It should also be pointed out that Eq. 7 has several shortcomings. For example, it is seen in Fig. 5 that while the Eq. 7 provides a good fit to the experimental data up to 1 mM NaCl, it falls of much quicker than the experimental data at higher concentrations. The reason for this could be that at higher concentrations the simple electrical double layer model presented becomes inaccurate. According to the model leading to Eq. 7, additivity of the two terms Q_0 and ΔQ is assumed, which means that the total charge transferred should become Q_0 for sufficiently high salt concentrations. However, it is observed that for concentrations of 1 M NaCl and above, the transferred charge becomes smaller than that for pure water. The origin of this reduction is not known, but it is possible that only in larger salt concentrations ions contribute to efficient screening of the surface charge sites that provide the charge transfer Q_0 in pure water. In such a picture will not only the electrical double layer be so thin that no ions are removed from the diffuse double layer by flow, they will also swarm the surface charge sites formed by contact with water and screen them out. The author has also found that it is possible to obtain a much better fit of Eq. 7 to the experimental data at high salt concentrations by letting x_s vary between a few nanometers to several hundred nanometers for different high concentrations. However, the author is not aware of any experimental data or simulations that justify such a large span in the stagnant layer, thus making such variations unlikely. A more elaborate model taking into account the interaction between charged species as well as reasonable variations in the stagnant layer in order to provide a better fit to the experimental data is needed to understand the charge transfer at high salt concentrations.

Despite the lack of quantitative agreement with experimental data at large concentrations, the proposed theoretical explanation of the experimental data is sufficiently simple and successful to suggest that the enhanced charge transfer is indeed governed by ions in the double layer. That is, the origin of the charge enhancement can be explained by a ‘streaming effect’ whereby the ions in the diffuse part of the electrical double layer contribute to the facilitation of contact electrification as long as the ion concentration is low. At higher concentrations, the double layer may contract more than the stagnant layer, such that fewer ions are removed resulting in smaller charge transfer due to triboelectrification. The arguments presented in

the current work should also be applicable to the data presented in Refs. [56-58], where it is likely that the charge enhancement is facilitated by ions in the double layer, and that the reduction in charge at larger ion concentrations is due to double layer screening. It should be mentioned that this work only studied the charge enhancement and reduction due to additional salt ions, and that the mechanism for the underlying contact electrification for pure water has not been identified.

Conclusion

In this study, it has been found that a new type of double-electrode device with one electrode exposed to water can be used to harvest energy by dipping it into water. When a small amount of salt is added to the water solution to obtain a concentration of 0.1-1 mM, the charge, current and electrical power transferred to an external load is found to increase significantly. A simple model to explain this behavior is suggested based on removal of charge from the diffuse electrical double layer of the hydrophobic surface, and found to fit well with experimental data at small salt concentrations. At larger concentrations exceeding 1 mM the simple model suggests a too strong screening compared to the experimental data, and it is likely that one has to account for the interactions and screening between different charged species to be able to explain the observed charge transfer decay.

REFERENCES

(1) W. Thomson, "On a self-acting apparatus for multiplying and maintain electric charges, with applications to illustrate the voltaic theory", Proc. R. Soc. London **1867**, 16, 67-72, available at http://www.jstor.org/stable/112474.

(2) Z. Levin, and P.V. Hobbs, "Splashing of Water Drops on Solid and Wetted Surfaces: Hydrodynamics and Charge Separation", Philos. Trans. R. Soc. A. **1971**, 269, 555-585.

(3) J.K. Beattie and A.M. Djerdjev, "The pristine oil/water interface: surfactant-free hydroxide-charged emulsions", Angew. Chem. Int. Ed., **2004**, 43, 3568-3571.

(4) I. Langmuir, "Surface electrification due to recession of aqueous solutions from hydrophobic surfaces", J. Am. Chem. Soc., **1938**, 60, 1190-1194

(5) G.H. Pollack, "The Fourth Phase of Water Beyond Solid, Liquid, and Vapor", Ebner&Sons, **2013**.

(6) P. Creux, J. Lachaise, A. Garcia, J.K. Beattie and A.M. Djerdjev, "Strong specific hydroxide ion binding at the pristine oil/water and air/water interfaces", J. Phys. Chem. B, **2009**, 113, 14146-14150

(7) M. Chaplin, Water, "Theory vs. experiment: What is the surface charge of water", **2009**, 1, 1-28.

(8) M. Kowacz and G.H. Pollack, "Moving water droplets: The role of atmospheric CO_2 and incident radiant energy in charge separation at the air-water interface", J. Phys. Chem. B, **2019**, 123, 11003-11013.

(9) L.P. Santos, T.R.D. Ducati, L.B.S. Balestrin and F. Galembeck, "Water with excess electric charge", J. Phys. Chem. C, **2011**, 115, 11226-11232.

(10) R. Williams, “The relation between contact charge transfer and chemical donor properties”, J. Coll. Int. Sci., **1982**, 88, 530-535.

(11) T.A.L. Burgo, F. Galembeck and G.H. Pollack, “Where is water in the triboelectric series”, J. Electrostatics, **2016**, 80, 30-33.

(12) Y. Sun, X. Huang and S. Soh, “Solid-to-liquid charge transfer for generating droplets with tunable charge”, Angew. Chem. Int. Ed., **2016**, 55, 9956-9960.

(13) I. Langmuir, “Surface electrification due to recession of aqueous solutions from hydrophobic surfaces”, J. Am. Chem. Soc., **1938**, 60, 1190-1194

(14) V.V. Yaminsky, M.B. Johnston, “Static electrification by nonwetting liquids. Contact charging and contact angles”, Langmuir, **1995**, 11, 4153-4158.

(15) M. Matsui, N. Murasaki, K. Fujibayashi, P.Y. Bao and Y. Kishimoto, “Electrification of pure water flowing down a through set up with a resin sheet”, J. Electrostatics, **1993**, 31, 1-10.

(16) K. Yatsuzuka, Y. Mizuno and K. Asano, “Electrification phenomena of pure water droplets dripping and sliding on a polymer surface”, J. Electrostatics, **1994**, 32, 157-171.

(17) R. Zimmermann, S. Dukhin and C. Werner, “Electrokinetic measurements reveal interfacial charge at polymer films caused by simple electrolyte ions”, J. Phys. Chem. B, **2001**, 105, 8544-8549.

(18) J.K. Beattie, “The intrinsic charge on hydrophobic microfluidic substrates”, Lab Chip, **2006**, 6, 1409-1411.

(19) K.N. Kudin, R. Car, “Why are water-hydrophobic interfaces charged”, J.Am. Chem. Soc., **2007**, 130, 3915-3919.

(20) M.D. Baer, I.F.W. Kuo, D.J. Tobias and C.J. Mundy, “Towards a unified picture of the water self-ions at air-water interface: A density functional theory perspective”, J. Phys. Chem. B, **2014**, 118, 8364-8372.

(21) S. Strazdaite, J. Versluis and H.J. Bakker, “Water orientation at hydrophobic interfaces”, J. Chem. Phys., **2015**, 143, 084708.

(22) A.Z. Stetten, D.S. Golovko, S.A.L. Weber and H.J. Butt, “Slide-electrification: charging of surfaces by moving water drops”, Soft Matter, **2019**, 15, 8667-8679.

(23) B. He and A. Darhuber, “Electrical surface charge patterns induced by droplets sliding over polymer and photoresist surfaces”, J. Micromech. Microeng., **2019**, 29, 105002.

(24) J.F. Osterle, “Electrokinetic energy conversion”, J. Appl. Mech., **1964,** 31, 161-164.

(25) W. Olthuis, B. Schippers, J. Eijkel and A. van den Berg, "Energy from streaming current and potential", Sensors and Actuators B **2005**, 111-112, 385-389.

(26) A.M. Duffin and R.J. Saykally, “Electrokinetic power generation from liquid water microjets”, J. Phys. Chem. C **2008**, 112, 17018-17022.

(27) A.G. Marin, W. van Hoeve, P. Garcia-Sanchez, L. Shui, M.A. Fontelos, J.T. Eijkel, A. van den Berg and D. Lohse, “The microfluidic Kelvin water dropper”, Lab Chip **2013**, 13, 4503-4506.

(28) J. K. Moon, J. Jeong, D. Lee, and H. K. Pak, “Electrical power generation by mechanically modulating electrical double layers” Nat. Commun. **2013**, 4, 1487.

(29) Z.H. Lin, G. Cheng, L. Lin, S. Lee and Z.L. Wang, “Water-solid surface contact electrification and its use for harvesting liquid wave energy”, Angew. Chem. Int. Ed. **2013**, 52, 1-6.

(30) S.-H. Kwon, J.W. Park, W.K. Kim, Y. Yang, E. Lee, C.J. Han, S.Y. Park, J. Lee and Y.S. Kim, "An effective energy harvesting method from a natural water motion active transducer", Energy Environ. Sci., **2014**, 7, 3279-3283.

(31) Z.H. Lin, G. Cheng, S. Lee, K.C. Pradel and Z.L. Wang, "Harvesting water drop energy by sequential contact electrification and electrostatic induction process", Adv. Mater **2014**, 26, 4690-4696.

(32) L. Zheng, Z.H. Lin, G. Cheng, W. Wu, X. Wen, S. Lee and Z.L. Wang, "Silicon-based hybrid cell for harvesting solar energy and raindrop electrostatic energy", Nano Energy, **2014**, 9, 291-300.

(33) Q. Liang, X. Yan, Y.Gu, K. Zhang, M. Liang, S. Liang, X. Zheng and Y. Zhang, "Highly transparent triboelectric nanogenerator for harvesting water-related energy reinforced by antireflection coating", Scientific Reports, **2015**, 26, 4690-4696.

(34) S.B. Jeon, D. Kim, G.-W. Yoon, J.-B. Yoon and Y.-K. Choi, "Self-cleaning hybrid energy harvester to generate power from raindrop and sunlight", Nano Energy, **2015**, 12, 636-645.

(35) G. Zhu, Y. Su, P. Bai, J. Chen, Q. Jing, W. Yang and Z.L. Wang, 'Harvesting water wave energy by asymmetric screening of electrostatic charges on a nanostructured hydrophobic thin-film surface', ACS Nano, **2014**, 8, 6031-6037.

(36) J. Han, B. Yu, G. Qu, H. Chen, Z. Su, M. Shi, B. Meng, X. Cheng and H. Zhang," Electrification based devices with encapsulated liquid for energy harvesting, multifunctional sensing, and self-powered visualized detection", J. Mater. Chem. A, **2015**, 3, 7382-7388.

(37) D. Choi, S. Lee, S.M. Park, H. Cho, W. Hwang and D.S. Kim, "Energy harvesting model of moving water inside a tubular system and its application of a stick-type compact triboelectric nanogenerator", Nano Research, **2015**, 3, 7382-7388.

(38) J.W. Park, Y. Yang, S.-H. Kwon and Y.S. Kim, “Influences of surface and ionic properties on electricity generation of an active transducer driven by water motion”, J. Phys. Chem. Lett., **2015**, 6, 745-749.

(39) L.E. Helseth and X.D. Guo, “Contact electrification and energy harvesting using periodically contacted and squeezed water droplets”, Langmuir, **2015**, 31, 3269-3276.

(40) Y. Sun, X. Huang and S. Soh, “Using the gravitational energy of water to generate power by separation of charge at interfaces”, Chem. Sci., **2015**, 6, 3347-3353.

(41) L.E. Helseth and X.D. Guo, “Hydrophobic polymer covered by a grating electrode for converting the mechanical energy of water droplets into electrical energy”, Smart. Mat. Struct., **2016**, 25, 045007.

(42) L.E. Helseth, “Electrical energy harvesting from water droplets passing a hydrophobic polymer with a metal film on its back side”, J. Electrostat., **2016**, 81, 64-70.

(43) X. Yang, S. Chan, L. Wang and W.A. Daoud, “Water tank triboelectric nanogenerator for efficient harvesting of water wave energy over a broad frequency range”, Nano Energy, **2018**, 44, 388-398.

(44) J.W. Lee and W. Hwang, “Theoretical study of micro/nano roughness effect on water-solid triboelectrification with experimental approach”, Nano Energy, **2018**, 52, 315-322.

(45) Y. Liu, Y. Zheng, T. Li, D. Wang and F. Zhou, “Water-solid triboelectrification with self-repairable surfaces for water-flow energy harvesting”, Nano Energy, **2019**, 61, 454-461.

(46) J. W. Park, S. Ong, C.H. Shin, Y.Y. Yang, S.A.L. Weber, E. Sim and Y.S. Kim, “Ion specificity on electric energy generated by flowing water droplets”, Angew. Chem. Int. Ed., **2018**, 57, 2091-2095.

(47) Y. Song, B. Xu, Y. Yuan, H. Xu and D. Li, "Coalescence of a water drop with an air-liquid interface: Electric current generation and critical micelle concentration (CMC) sensing", ACS Appl. Mater. Interfaces, **2019**, 11, 16981-16990.

(48) G. Chen, X. Liu, S. Li, M. Dong and D. Jiang, "A droplet energy harvesting and actuation system for self-powered digital microfluidics", Lab Chip, **2018**, 18, 1026-1034.

(49) D. Jiang, M. Xu, M. Dong, F. Guo, X. Liu, G. Chen and Z.L. Wang, "Water-solid triboelectric nanogenerators: An alternative means for harvesting hydropower", Renewable and Sustainable Energy Reviews, **2019**, 115, 109366.

(50) W. Tang, B.D. Chen and Z.L. Wang, "Recent progress in power generation from water/liquid droplet interaction with solid surfaces", Advanced Functional Materials, **2019**, 1901069.

(51) L. Liu, Q. Shi, J.S. Ho and C.K. Lee, "Study of thin film blue energy harvester based on triboelectric nanogenerator and seashore IoT applications", Nano Energy, **2019**, 66, 104167.

(52) W. Xu, H. Zheng, X. Zhou, C. Zhang, Y. Song, X. Deng, M. Leung, Z. Yang, R.X. Xu, Z.L. Wang, X.C. Zeng and Z. Wang, "A droplet-based electricity generator with high instantaneous power density", Nature, **2020**, 578, 392-396.

(53) L.E. Helseth, "The influence of microscale surface roughness on water-droplet contact electrification", Langmuir, **2019**, 35, 8268-8275.

(54) P.W. Chudleigh, "Mechanism of charges transfer to a polymer surface by a conducting liquid contact", J. Appl. Phys., **1976**, 47, 4475-4482.

(55) L.E. Helseth and H.Z. Wen, "Visualisation of charge dynamics when water droplets move off a hydrophobic surface", Eur.J. Phys., **2017**, 38, 055804.

(56) L.E. Helseth, "A water droplet-powered sensor based on a charge transfer to a flow-through front surface electrode", Nano Energy, **2020**, 73, 104809.

(57) J.W. Park, Y.J. Yang, S.H. Kwon, S.G. Yoon and Y.S. Kim, "Analysis on characteristics of contact-area-dependent electric energy induced by ion sorption at solid-liquid interface", Nano Energy, **2017**, 42, 257-261.

(58) J. Nie, Z. Ren, L. Xu, S. Lin, F. Zhan, X. Chen and Z.L. Wang, "Probing contact-electrification-induced electron and ion transfers at a liquid-solid interface", Adv. Mater., **2020**, 32, 1905696.

(59) E. Poli, K.H. Jong and A. Hassanali, "Charge transfer as a ubiquitous mechanism in determining the negative charge at hydrophobic interfaces", Nature Commun., 2020, 11, 901.

(60) R.J. Hunter, "Introduction to modern colloid science", Oxford Science Publications, 1st ed., **1993**.

(61) S.R. Maduar, A.V. Belyaev, V. Lobaskin and O.I. Vinogradova, "Electrohydrodynamics near hydrophobic surfaces", Phys. Rev. Lett., **2015**, 114, 118301.

(62) R. Hartkamp, A.L. Biance, L. Fu, J.F. Dufrêche, O. Bonhomme and L. Joly, "Measuring surface charge: Why experimental characterization and molecular modelling should be coupled", Current Opinion in Colloid & Interface Science, **2018**, 37, 101-114.

(63) P. Khan, J. Chakraborty and S. Chakraborty, "Electrokinetics over hydrophobic surfaces", Electrophoresis, **2019**, 40, 616-624.

(64) R. Kou, Y. Zhong and Y. Qiao, "Effects of anion size on flow electrification of polycarbonate and polyethylene terephthalate", Appl. Phys. Lett., **2019**, 115, 073704.

For Table of Contents Use Only